JOURNAL OF AIRCRAFT
Vol. 33, No. 2, March–April 1996

Subsonic Aerodynamics and Performance of a Smart Vortex Generator System

Ron Barrett*
Auburn University, Auburn, Alabama 36849-5338
and
Saeed Farokhi†
University of Kansas, Lawrence, Kansas 66045-2221

A new system for active flow control using smart vortex generators (SVG) is presented. Increments in $C_{l\max}$ from modern vortex generators (VGs) are determined through wind-tunnel testing on a two-dimensional wing section. Using an optimized VG configuration, a system was built with 1) a shear-flow sensor that detected the onset and depth of stall, 2) a series of shape-memory-alloy VGs, and 3) a lift-to-drag (*L/D*) maximizing controller. The system demonstrated a 14% increase in $C_{l\max}$, a 2.7-deg rise in α_{stall}, a 42% jump in *L/D* through the stall, and a low α C_{d0} penalty of less than 0.1%. Further testing demonstrated that the system consumed only 9.2 W of power, responded in less than 0.8 s, and was capable of unstalling an airfoil that had exceeded α_{stall} by up to 3 deg.

Nomenclature

C_d = two-dimensional drag coefficient
C_l = two-dimensional lift coefficient
c = chord
d = lateral vortex generator spacing
h = height of vortex generator, normal to airfoil
l = length of vortex generator, chordwise
r = streamwise distance from tip of vortex generator
w = spanwise width of vortex generator
α = angle of attack of wing section
δ = deflection of plate vortex generator above surface

I. Introduction

FOR more than 50 years, airplanes, ships, and ground vehicles have used vortex generators (VGs) for performance enhancement. Modern VGs are frequently used to reattach separated flow, improve control characteristics, decrease transonic drag, and generally fine-tune aircraft performance in a specific flight regime.[1] The most common type are vane VGs that can be found on many commercial airliners and general aviation aircraft like the Beech Starship that uses vane VGs on the wings, canards, and vertical stabilizers.[2] Frequently, VGs are used to increase $C_{l\max}$ and lower aircraft stall speed.[3] Unfortunately, these devices also cause a significant increase in drag over the clean configuration during cruise.

Accordingly, methods of maintaining the increase in $C_{l\max}$ while incurring no increase in C_{d0} are highly desirable. A partial solution is to use new types of lift enhancement devices. One new type of advanced vortex generator employs the Wheeler configuration (Fig. 1) to induce attached flow at significantly reduced drag penalties of only 2–4% C_{d0}.[4–8]

Another system of flow control through vortex manipulation uses air jets blown tangentially to the freestream. McFadden[9] and Johnston and Nishi[10,11] showed that air jets can generate vortices that are strong enough to facilitate flow attachment. Although this arrangement did produce an increase in $C_{l\max}$ without incurring a significant rise in C_{d0}, system complexity, weight, and power consumption were high.

In an effort to solve these problems while maintaining the aerodynamic benefits, different types of folding VGs have been examined. Vess[12] and Örnberg[13] proposed using conventional vane VGs with hinges at the base that would be extended at high α and retracted during cruise. Unfortunately, these active vane VGs require cutouts in the wing skin, and sizable, internally mounted actuator devices that are necessary to counter large aerodynamic hinge moments.

In the 1950s, Stephens and Collins[14,15] explored wedge and ramp VGs. They proposed that the wedges or ramps be raised or lowered as required for flow attachment. This configuration is more amenable to extension and retraction than the folding vane VG, because the hinge moments about the base are one to two orders of magnitude lower, and the simple form allows for efficient collapse and activation with close surface conformity. Figure 1 shows the geometry of the Stephens and Collins VGs in the singlet and doublet (Wheeler) configurations.

Because the wedge and ramp VGs generally induce a lower drag penalty than the vane-type VGs for a given height, much larger sizes are frequently used, which leads to even greater increments in $C_{l\max}$. In the 1980s, a series of experiments with

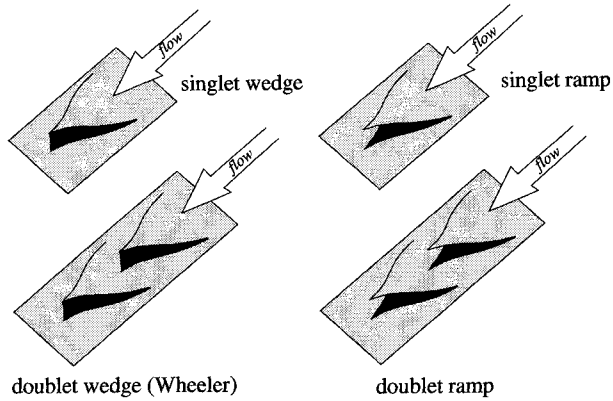

Fig. 1 Ramp and wedge VG configurations.

Received Oct. 2, 1994; revision received Sept. 15, 1995; accepted for publication Oct. 10, 1995.

*Assistant Professor, Aerospace Engineering Department, 211 Aerospace Engineering Building. Member AIAA.
†Professor and Director of the Flight Research Laboratory, Nichols Hall. Associate Fellow AIAA.

cascaded wedge VGs in excess of 50%c in length, demonstrated that $C_{l\max}$ could be increased by as much as 40% over the clean wing configuration.[5,8]

The primary goal of this study will be to demonstrate the utility of a lift enhancement system that will generate a significant increase in α_{stall} and $C_{l\max}$ while inducing a negligible rise in C_{d0} with very little weight and power consumption. The present study will draw upon earlier smart VG work[16] and use 1) the ramp VG configuration with shape-memory-alloy (SMA) actuators, 2) a shear-flow stall sensor, and 3) an optimal controller. These three components will be combined to form a smart vortex generator (SVG) system that will optimize lift-to-drag (L/D) and $C_{l\max}$ as a function of angle of attack.

II. Design, Construction, and Testing of the SVG System

The evaluation of the SVG system was accomplished in three major stages:

1) The shape, size, chordwise position, and spanwise spacing of the ramp VGs were determined experimentally so that the greatest increase in $C_{l\max}$ would be achieved with small-span VGs.

2) The SMA actuators, shear flow sensor, and controller were designed, built, and integrated in the wing section.

3) The entire arrangement was wind-tunnel tested so that appropriate controller gains could be set and closed-loop performance could be evaluated.

A. Optimum Configuration Selection of Static Ramp VGs

The first task of the investigation was to determine the shape, type, size, and geometric pattern of the VGs on the airfoil surface that would optimize $C_{l\max}$. From the work of Wheeler[5,7,8] and Barrett[16] it was shown that the optimal ramp VG shape has a curvature similar to the upper section of an ellipse with an aspect ratio l/w from 1 to 2 as shown in Fig. 2.

Further investigation showed that the $C_{l\max}$ increase from the doublet VGs is virtually the same as induced by the singlet VGs (within 0.5%).[16,17] Accordingly, the singlet configuration was selected for simplicity.

The next geometric parameter to be selected was the physical size of the VGs. This was accomplished through a series of wind-tunnel tests in the 42 in. (107 cm) × 50 in. (127 cm) at the University of Kansas Subsonic Wind Tunnel, which is a closed-circuit return type with a turbulence factor of 1.1 (as defined by Rae and Pope[18]).

A NACA 4415 airfoil section was constructed from a wood core with a polyester resin finish with a chord of 8 in. and a reference area S_{ref} of 200 in.^{2}. The surface tolerance was kept to within 3.5 mil (89 μm) of the prescribed profile and was finished with 600-grit paper and ultrafine ScotchBrite pads.® The two-dimensional model was mounted between 32 in. (81.3 cm) × 30 in. (76.2 cm) splitter plates with crossflow baffles. Lift was measured using a six-component balance, and drag measurements were taken using a wake rake. The airfoil was tested at a Reynolds number of 4.27×10^4 at 100 ft/s (30.5 m/s) with 0.004-in.- (102-μm-) diam roughness applied to the first 8%c as recommended in Ref. 18.

Three different sizes of VGs were tested on the wing section: 0.5 in. (12.7 mm), 1 in. (25.4 mm), and 1.5 in. (38.1 mm) in span. From earlier studies on similar wing sections, it was determined that the ramp VGs are most effective when placed 5–15% behind the leading edge.[5,8,16] The configuration testing was conducted with the VGs placed just behind the trip strip at 8% c. Figure 3 shows a typical VG arrangement on the test article.

Table 1 lays out the test matrix that was used to determine the optimum vortex generator size and configuration.

The wind-tunnel data exhibited excellent repeatability as 100 samples were taken at each point. The 99% confidence intervals are shown, but fall within the plot symbols. Figure 4 includes corrections to C_l using the procedures of Ref. 19 and shows excellent agreement with the baseline data published in Ref. 20 (within 2%). At high angles of attack, beyond the stall, significant deviations from published data were originally present because of a system harmonic, but were removed using a 15-Hz low-pass filter.

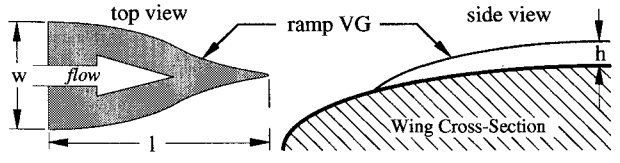

Fig. 2 Geometry of typical ramp VG.

Table 1 Test matrix for VG configuration and sizing study

VGs per row	VG size, in.	Type	Row placement, % c
24	0.5 × 0.5	Singlet	8
24	0.5 × 0.5	Doublet	8
12	0.5 × 0.5	Singlet	8
12	1 × 1	Singlet	8
6	1 × 1	Singlet	8
6	1 × 1	Doublet	8
6	1.5 × 1.5	Doublet	8

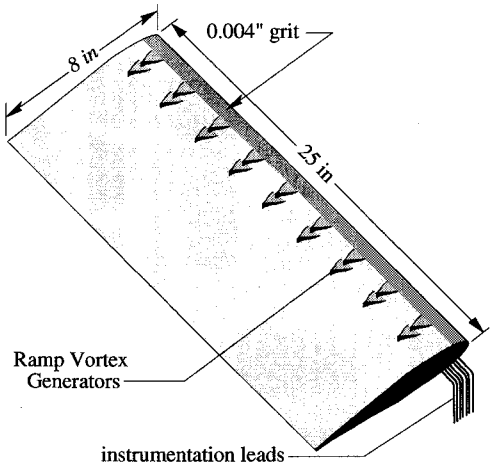

Fig. 3 Arrangement of VGs on wing section.

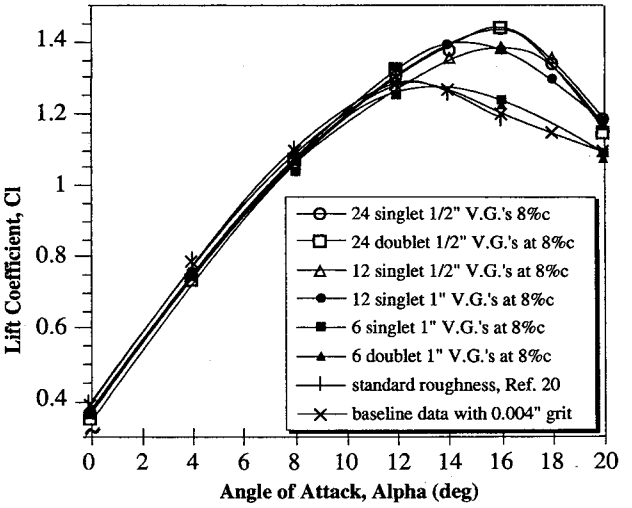

Fig. 4 Vortex generator sizing wind-tunnel data.

As can be seen in Fig. 4, the use of the scaled roughness of 0.004-in.-diam grit at a Reynolds number of 4.27×10^4 resulted in section performance that was nearly identical (within 2%) to the standard roughness NACA 4415 of Ref. 20, which was tested at a Reynolds number of 6×10^7. Accordingly, the effects of the disparity in Reynolds number have been effectively offset through the use of the scaled leading-edge roughness.

Figure 5 shows the test results from the sizing experiments in terms of $C_{l\max}$. It is clear that the largest lift increase occurs at the closer spacing, and that the 1-in. (25.4-mm) and 0.5-in. (12.7-mm) VGs perform similarly, except that the smaller VGs allow for more per row. Accordingly, the $\frac{1}{2}$-in. VGs were chosen over the larger VGs.

After the selection of the 0.5-in. (12.7-mm) VG size, the next optimization parameter was the chordwise position of the VGs. The test matrix includes two different center-to-center spacings of $d = 1$ in. (25.4 mm) and 1.5 in. (38.1 mm), with the VGs placement varied from 8 to 90% c behind the leading edge as shown in Table 2.

The test results are displayed on a contour plot to show the region of maximum lift generation clearly (again, the 99% confidence intervals fell within one line width). Figures 6 and 7 clearly show that the highest $C_{l\max}$ is induced when the VGs are placed between 8–15% c behind the leading edge (as suggested in Refs. 5, 8, and 16).

The data of Fig. 6 show that when the VGs are placed beyond 40% c, they have virtually no effect on $C_{l\max}$. This is because of the trailing-edge stall that works its way forward with increasing α. This can clearly be seen in the flow visualization results of Ref. 16 as the separation line moves forward from approximately 80–85%c at low angles of attack to 15–20%c as α approaches the stall. From the shape of the lift-curve slope, the airfoil actually encounters a form of mixed stall; however, with VGs present, some leading-edge stall characteristics become more pronounced as shown in Fig. 7, which has a higher peak in $C_{l\max}$ than Fig. 6 (and the baseline data), followed by a steeper dropoff.

Table 2 Test matrix for chordwise placement study at 1.0- and 1.5-in. center-to-center spanwise spacing

VGs per row		VG size,		Row placement,
d = 1.0 in.	d = 1.5 in.	in.	Type	%c
24	16	0.5 × 0.5	Singlet	8
24	16	0.5 × 0.5	Singlet	10
24	16	0.5 × 0.5	Singlet	20
24	16	0.5 × 0.5	Singlet	30
24	16	0.5 × 0.5	Singlet	40
24	16	0.5 × 0.5	Singlet	50
24	16	0.5 × 0.5	Singlet	60
24	16	0.5 × 0.5	Singlet	70
24	16	0.5 × 0.5	Singlet	80
24	16	0.5 × 0.5	Singlet	90

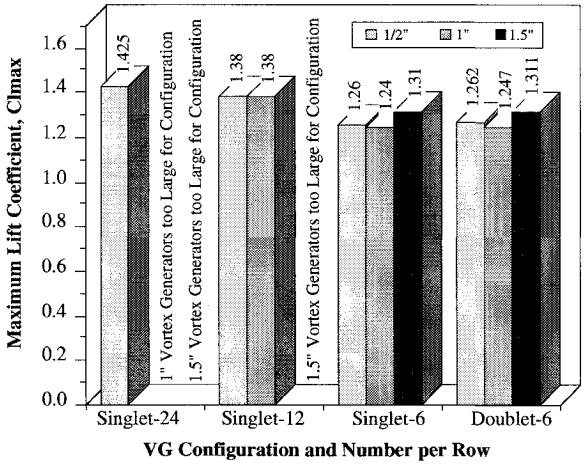

Fig. 5 Lift increase from VGs of different sizes.

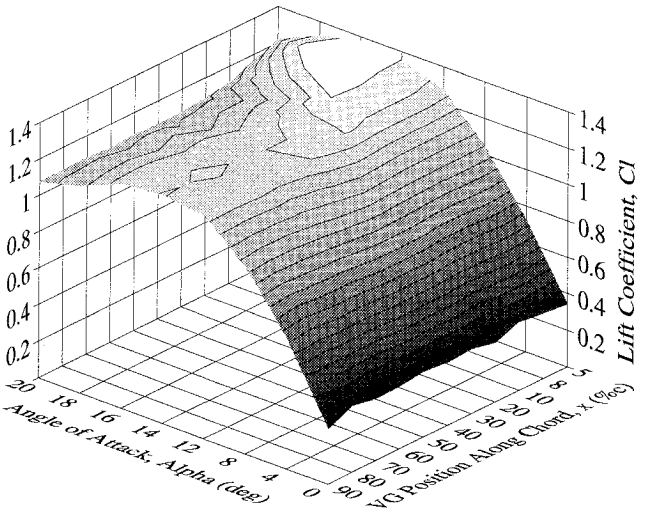

Fig. 6 Effect of VG chordwise position on C_l, d = 1.5 in.

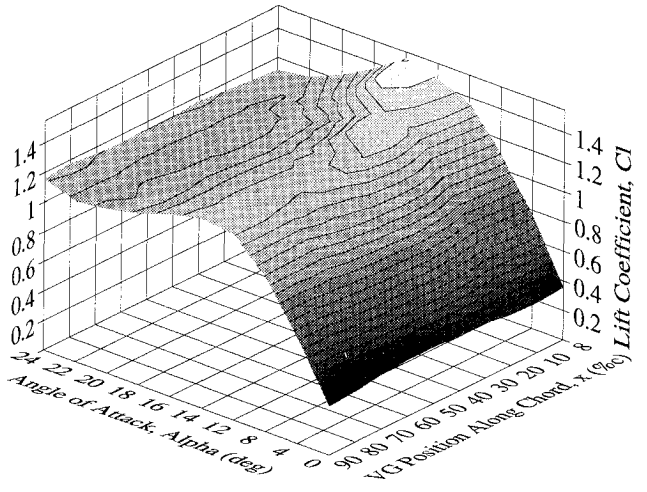

Fig. 7 Effect of VG chordwise position on C_l, d = 1.0 in.

B. Design and Construction of Ramp Vortex Generators and SMA Actuators

From Figs. 6–8, the optimum chordwise position of the VGs is between 8–15%c, at a spanwise spacing from 0.70 to 1.1 in. Using this data, a smart VG system was built with ramp VGs and SMA actuators, a shear-flow sensor, and an optimum controller. A schematic of the VGs and the shear-flow sensor is shown in Fig. 9.

The first components of the smart VG system to be designed were the ramp VGs themselves. Because significant lift enhancement has been shown with a variety of curvatures similar to that of the side view shown in Fig. 2, the VG profiles were selected to conform to the surface contour of the wing section [within 0.001 in. (25.4 μm)]. The surface conformity was verified by using a dial feeler gauge attached to the stationary component of a precision mill. The gauge system was accurate to 0.10 mil (2.54 μm). Using this profile, a rudimentary aero-

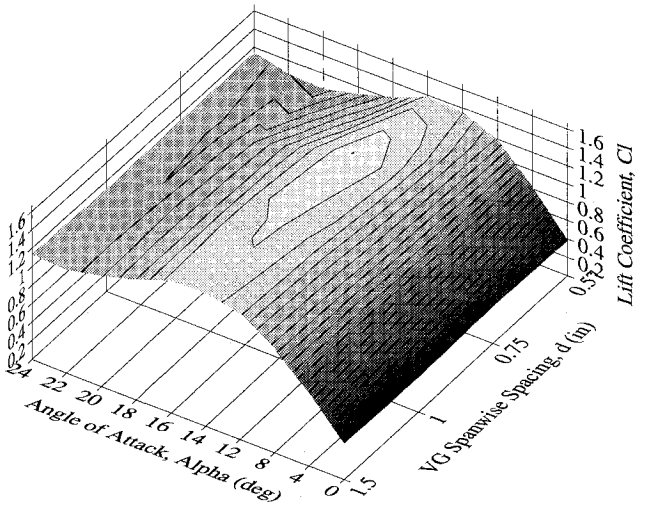

Fig. 8 Effect of spanwise spacing on C_l, with VGs at 8% c.

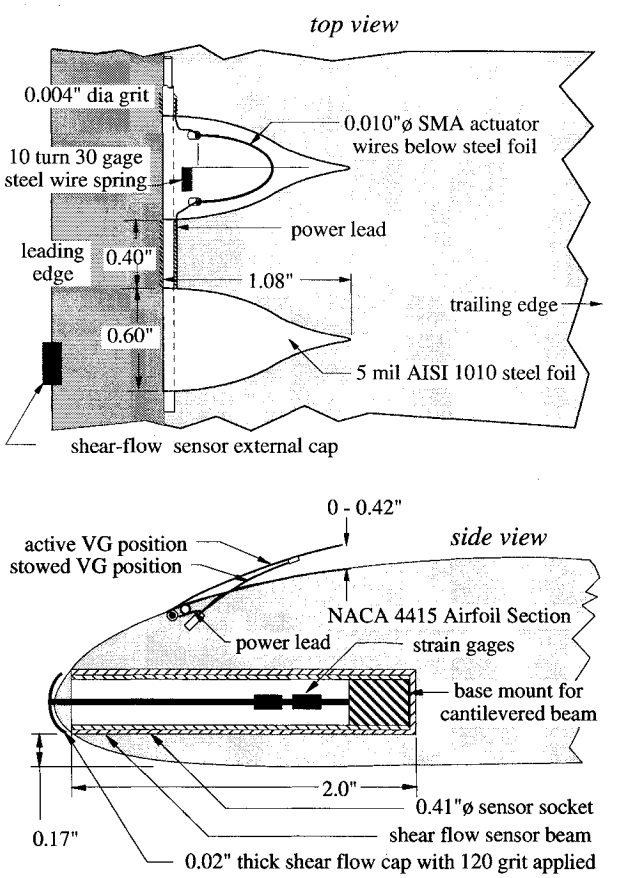

Fig. 9 Ramp VG and SMA actuator filament arrangement.

dynamic force estimation was made using strip aerodynamic theory at 100 ft/s under standard sea-level conditions, with a maximum deflection of 45 deg to the freestream. Assuming the base to be cantilevered and allowing a deflection of no more than 0.010 in. (254 μm), a 0.005-in.- (127-μm-) thick AISI 1010 steel ramp was chosen.

Beneath the steel ramp, SMA actuators were laid out. These actuator filaments were constructed from 0.010-in.- (254-μm-) diam Tinel alloy K nickel–titanium SMA and were to raise the ramps to 60 deg under no loading conditions, 30 deg at 100 ft/s. As with most SMAs, Tinel alloy K in its martensitic (cold) phase has a very low equivalent elastic modulus, below 1.5 msi (10 GPa). As it is heated above the transition temperature, it gains an austenitic modulus up to 8.7 msi (60 GPa). Active strains range from 1 to 8% in the normal working range. Between the change in moduli and active strain levels, useful work may be performed by the SMA actuator. Tinel alloy K actuators have performance typical of multicycle or motor shape-memory alloys. This is because they produce active strain levels that are typical of most alloys of this type, and yet suffer from less pronounced actuation fatigue. Using the Cosmos™ finite element code and data from Ref. 20 on local Cp distribution along the leading-edge of the airfoil, a ramp VG with a loop actuator filament was designed (Fig. 9). The reader is referred to Ref. 16 for more details on the design process as space constraints prohibit its detailed inclusion.

The next component of the system to be laid out was the shear-flow sensor that used a pair of temperature-compensated strain gauges bonded to a high-damping, low-density polyester beam, which was mounted within the leading edge of the section. The end of the beam had a rounded 0.20-in.- (5.1-mm-) square cap that protruded from the leading edge by 0.020 in. (508 μm) and was covered with 0.004-in. (102-μm) grit. As the flow passed over the grit-covered end, the beam was bent and the resistance of the sensor was changed.

Connected to the shear-flow beam was a controlling network constructed from a pair of Apex μTechnologies PA-26 high-current amplifiers, a signal chopper, and relays. A TL 555 timer chip chopped the signal at a rate of 4 Hz, which allowed for accurate relay control at high α. Gain adjusting potentiometers were used between the PA-26 inverting input and output to allow scheduling of the height of the VGs as a function of depth of stall.

The system was tested open loop and it was found that the actuators could reach a high operational height of $h = 0.22$ in. (5.6 mm) (see Fig. 2) within 0.8 s while consuming 2.14 A at 4.3 volts direct current (VDC) (9.2 W). Further open-loop testing revealed that the Tinel Alloy K actuators were capable of maintaining more than 99% of the original performance for more than 1200 cycles. This absence of actuator fatigue is because local filament strain rates were kept below 1%. A typical filament operational temperature was approximately 190°F with the surface of the ramp experiencing temperatures of only 110–120°F during steady operation at 0 ft/s airspeed.

C. Determination of Controller Gains and Closed-Loop SVG System Performance

After design, construction, and open-loop testing of the SVG network, the system gains for optimal scheduling of the ramp VGs as a function of α were determined. This was done by wind-tunnel testing for L/D as a function of VG height. Figure 10 shows VG height as a function of α for the generation of maximum L/D as well as the resulting SVG lift-curve slope. The controller system gains were adjusted to match the height profile of Fig. 10 within 3%h. Below 10.5 deg, the VGs were retracted flat to the surface with a maximum height of 0.006 in. (152 μm) at the trailing edge of the VGs.

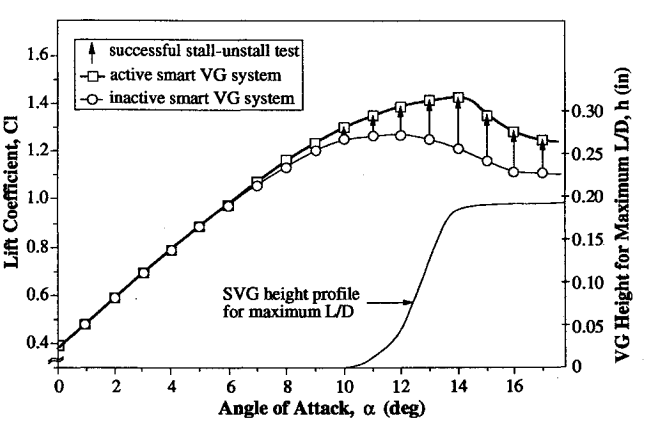

Fig. 10 Lift curve and deflection schedule for SVG system.

Using the optimum deflection schedule, a series of tests were conducted with the system off, system on, and the system cycled off, then on to show that a stalled wing may be unstalled by smart VGs. Figure 10 also shows the $C_l-\alpha$ curve for the wing with the system off, which deviates less than 3% from the NACA 4415 standard roughness data of Ref. 20.

The vertical lines between the upper and lower $C_l-\alpha$ curves represent unstall test sequences that consisted of 1) set α to a specified angle of attack with the SVG system off; 2) wait 1 min to take 100 data points (at 50 samples/s) with retracted VGs; 3) turn on the SVG system, which raised the VGs within 0.8 s; and 4) immediately after the VGs reached full deflection, take 100 samples. Although the wind tunnel operated at a turbulence factor of 1.1, numerous unstall tests were conducted at speeds as low as 40 ft/s (12.2 m/s) (Reynolds number = 170.8×10^3), and as high as 150 ft/s (45.7 m/s) (Reynolds number 640.5×10^3) with trends that mirror the results of Fig. 10.

In addition to matching the standard roughness $C_l-\alpha$ data of Ref. 20, the drag data of the wing section with the SVG system off also fell within 3%. Using wake-rake measurements, the increase in drag because of the presence of retracted VGs over the clean wing without VGs was less than 0.1% C_{d0}, which was the limit of resolution for the instrumentation.

Wind-tunnel testing also demonstrated significant reductions in drag as well as an increase in lift through the stall as seen in the drag polar of Fig. 11. From 10–13 deg α, the activated SVG system generated more lift than the clean wing (or inactive SVG system) configuration while simultaneously producing less drag than the fully extended VG configuration. This is because of partial VG deflection following the schedule of Fig. 10.

From Fig. 9 it can also be seen that a return-force spring was also used. This spring tightly pulled the ramp VG to the surface of the wing at low α. Accordingly, the maximum VG protrusion above the wing surface was 0.006 in. (152 μm) at the trailing edge of the VG when stowed. The leading edge of the ramp VGs were trimmed to a thickness of 0.004 in. (102 μm), which means that the VGs were entirely within the boundary layer when retracted (recall 0.004-in.-diam grit to 8%c). This arrangement led to a negligible rise in C_{d0} during low α operation from 0.01150 to 0.01151 (this 0.1% change in C_{d0} is within the error band of the measuring device).

The increase in lift and decrease in drag beyond α_{stall} also induced a sizable jump in the lift-to-drag ratio. As seen in Fig. 12, *L/D* was boosted significantly in the 12–16 deg range. At 15 deg, *L/D* was more than 42% greater than the clean (inactive) configuration.

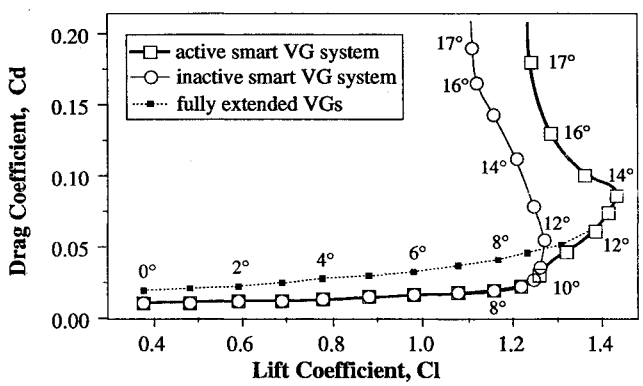

Fig. 11 Drag polar of the SVG system.

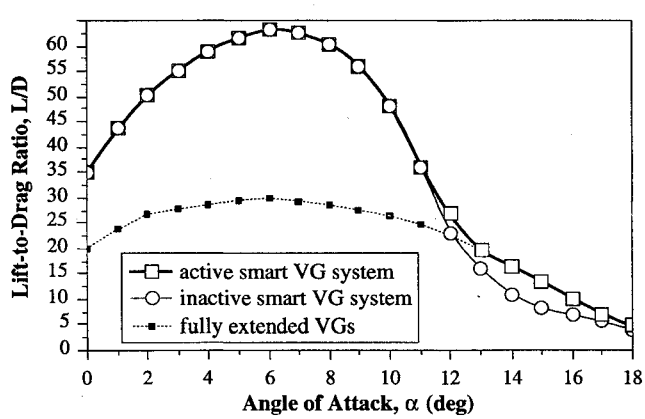

Fig. 12 *L/D* as a function of α for the SVG system.

III. Conclusions

Using a smart ramp vortex generator system and a NACA 4415 airfoil section with an 8-in. (20.3-cm) chord, the VG arrangement that provides the highest $C_{l\max}$ is 1) base VG width from 0.50 to 0.75 in., 2) placed 8–15%c behind the leading edge, and 3) spanwise spacing of 0.75–1.0 in.

Using smart ramp vortex generators, which were actuated by shape-memory-alloy (SMA) wire, and triggered by a leading-edge shear flow sensor and optimal controller, $C_{l\max}$ was raised from 1.26 to 1.43, α_{stall} was increased from 12.5 to 14.3 deg, and *L/D* gained as much as 42% above 12.5-deg α, while the wing section incurred a low α drag penalty under 0.1%.

The increase in $C_{l\max}$ afforded by the smart vortex generators could be achieved both by actuating the VGs at low α, then increasing α through the stall, or by keeping the VGs retracted through the stall, then actuating the VGs to unstall the wing.

Acknowledgments

The authors acknowledge the assistance and support of Aerotech Engineering and Research of Lawrence, Kansas, for directing this work under contract from the Kansas Technology Enterprise Corporation. The authors thank David Downing and NASA Headquarters for providing support through the Kansas Space Grant Consortium. The authors also thank Chris Hardin for making the wind-tunnel data acquisition system usable through his exceptionally useful and well-written codes.

References

[1]Taylor, H. D., "United Aircraft Research Department Summary Report on Vortex Generators," United Aircraft Corp., Research Dept., Rept. R-05280-9, East Hartford, CT, March 1950.

[2]Taylor, J. W. R., "USA Aircraft—Beech," *Jane's All the World's Aircraft*, Jane's Information Group, Ltd., Sentinel House, Couldson, Surrey, England, UK, 1989, pp. 324–336.

[3]Lan, C. E., and Roskam, J., "Wing Stall," *Airplane Aerodynamics and Performance*, Roskam Aviation and Engineering Corp., Ottawa, KS, 1980, pp. 111–116.

[4]Lin, J. C., and Howard, F. G., "Turbulent Flow Separation Control Through Passive Techniques," *AIAA 2nd Shear Flow Conference*, AIAA, Washington, DC, 1989 (AIAA Paper 89-0976).

[5]Wheeler, G. O., "Wheeler VG's," Vortex Products, Sumner, WA, 1989.

[6]Rao, D. M., and Kariya, T. T., "Boundary-Layer Submerged Vortex Generators for Separation Control—An Exploratory Study," AIAA Paper 88-3546, July 1988.

[7]Wheeler, G. O., "Means for Maintaining Attached Flow of a Flowing Medium," U.S. Patent 4,455,045, June 19, 1984.

[8]Wheeler, G. O., "Wind Tunnel Experimentation on a Modified Liebeck Airfoil," Vortex Products, Inc., Internal Rept., Sumner, WA, 1988.

[9]McFadden, R., "Attached Jet Spanwise Blowing Lift Augmentation System," U.S. Patent 4,860,976, Aug. 29, 1989.

[10]Johnston, J., and Nishi, M., "Vortex Generator Jets—A Means for Passive and Active Control of Boundary Layer Separation," *AIAA 27th Aerospace Sciences Meeting*, AIAA, Washington, DC, 1989 (AIAA Paper 89-0564).

[11]Johnston, J., and Nishi, M., "Vortex Generator Jets—Means for Flow Separation Control," *AIAA Journal*, Vol. 28, No. 6, 1990, pp. 629–634.

[12]Vess, R. J., "Strake Fence Flap," U.S. Patent 4,739,957, April

26, 1988.

[13]Örnberg, K. T., "Stabilizing the Vortices over a Thin Delta Wing," U.S. Patent 3,471,107, Oct. 7, 1969.

[14]Stephens, A. V., "Solid Boundary Surface for Contact with a Relatively Moving Fluid Medium," U.S. Patent 2,800,291, July 23, 1957.

[15]Stephens, A. V., and Collins, B. E., "Turbulent Boundary Layer Control by Ramps or Wedges," Australian Aeronautical Research Committee Rept. ACA-55, Sydney, Australia, May 1955.

[16]Barrett, R., "An Experimental Evaluation of Smart Tetrahedral Vortex Generators," Ph.D. Dissertation, Univ. of Kansas, Aerospace Engineering Dept., Lawrence, KS, May 1993.

[17]Barrett, R., and Farokhi, S., "On the Aerodynamics and Performance of Active Ramp Vortex Generators," *AIAA 11th Applied Aerodynamics Conference*, AIAA, Washington, DC, 1993 (AIAA Paper 93-3447).

[18]Rae, W. H., and Pope, A., "Instrumentation and Calibration of the Test Section, Model Force, Moment and Pressure Measurements, and Testing Procedure," *Low-Speed Wind Tunnel Testing*, Wiley, New York, 1984, pp. 99–343.

[19]Allen, H. J., and Vincenti, W. G., "Wall Interference in a Two-Dimensional-Flow Wind Tunnel, with Consideration of the Effect of Compressibility," NACA Rept. 782, 1944.

[20]Abbott, I. H., and Von Doenhoff, A. E., "Basic Thickness Forms, and Aerodynamic Characteristics of Wing Sections," *Theory of Wing Sections*, Dover, New York, 1959, pp. 309–687.